Chinese Chemical Letters 37 (2026) 111331

Contents lists available at ScienceDirect

Chinese Chemical Letters

journal homepage: www.elsevier.com/locate/cclet

Enabling guest-binding selectivity in hexahedral metal-organic cages *via* vertex modification

Tian Tan[a], Jiao Hu[a], Ya-Liang Lai[a], Xian-Chao Zhou[a], Yong-Zhen Tan[a], Mo Xie[a], Yong-Liang Huang[b], Chuang-Wei Zhou[a], Hao-Jie Zhang[a], Dong Luo[a,*], Xiao-Ping Zhou[a,*], Dan Li[a]

[a] *College of Chemistry and Materials Science, Guangdong Provincial Key Laboratory of Supramolecular Coordination Chemistry, Jinan University, Guangzhou 510632, China*
[b] *Department of Medicinal Chemistry, Shantou University Medical College, Shantou 515041, China*

ARTICLE INFO

Article history:
Received 11 March 2025
Revised 12 May 2025
Accepted 15 May 2025
Available online 15 May 2025

Keywords:
Metal-organic cage
Host-guest chemistry
Vertex modification
Anion binding
Pyrene

ABSTRACT

This work investigates the impact of vertex modification on the host-guest chemistry of a hexahedral Zn(II)-based metal-organic cage (MOC) **1** containing fluorinated components. Structural characterization *via* single-crystal X-ray diffraction (SCXRD), ^{1}H NMR, and electrospray ionization time-of-flight mass spectra (ESI-TOF MS) confirmed the low-symmetry hexahedral architectures of **1·NTf$_2$** and **1·OTf**, with fluorine atoms positioned at cage windows. ^{1}H/^{19}F NMR spectra of **1·NTf$_2$** and **1·OTf** showed slow-exchange binding behavior with external anions. **1·NTf$_2$** had a single set of peaks in the imine signal area, while **1·OTf** had two distinct groups of signals. Combined with competitive anion titration results, it can be inferred that NTf_2^- has a stronger binding affinity with the cage structure. Host-guest studies with pyrene (Py) and its hydrogenated analogs revealed complete displacement of OTf^- but not NTf_2^-, highlighting the superior binding strength of NTf_2^-. Comparative isothermal titration calorimetry (ITC) data showed reduced association constants for **1·OTf** with pyrene (Py) and its analogs 4,5,9,10-tetrahydropyrene (4H-Py) and hexadecahydropyrene (16H-Py) compared to **2·OTf**, attributed to electron-withdrawing fluorine substituents altering charge distribution, which was confirmed by the electrostatic potential analysis of the cage skeleton. These findings underscore how vertex functionalization modulates anion selectivity and guest-binding thermodynamics in MOCs, offering insights for designing tailored supramolecular hosts.

© 2026 Published by Elsevier B.V. on behalf of Chinese Chemical Society and Institute of Materia Medica, Chinese Academy of Medical Sciences.

Metal-organic cages (MOCs) with diverse nanocavities created through coordination directed self-assembly have been the subject of thorough research due to their unique characteristics [1–9]. These cages are capable of accommodating a range of guest species, making them valuable for tasks such as chemical separations [10–12], stable active species [13–15], catalysis [16–18], and drug delivery [19,20]. In order to achieve the above functions, it is crucial and challenging to cleverly utilize supramolecular interactions and spatial effects that affect the binding ability between host and guest species, such as electrostatic affinity, hydrogen bonding, π-stacking, solvent effect, and steric hindrance [21–23].

The ligand modification in MOCs is a common approach involving replacing specific ligand substituents in a rational manner, exploiting electronic or spatial effects to directly influence the structure and properties of the cages [24–28]. Previously reported examples show that MOC structures with different topological or symmetrical types can be constructed by appropriately replacing substituents [29–34]. For instance, Fujita *et al.* created a giant $M_{30}L_{60}$ icosidodecahedron by adjusting the flexibility of the ligand through modifications with different numbers of methyl groups [29]. Nitschke *et al.* reported the successful construction of two new $Cu^{I}{}_{12}L_8$ cages with different structures using similar subcomponents except for the substituents (*e.g.*, –H, –F and $-OCH_3$) in the components [34]. However, the predictability of MOC topological structure changes caused by local substituent modification is unclear, which poses a challenge for studying the structure-activity relationships of its subsequent host-guest chemistry. Some interesting studies have shown that by appropriate vertex modification while keeping the MOC topology unchanged, the host-guest properties of the cage cavity can be well controlled [35–39]. For example, the subcomponent exchange converted the Fe^{II} centers of a tetrahedral cage from high-spin to low-spin state by replacing 2-formyl-6-methylpyridine with 2-formylpyridine, endowing the cage

* Corresponding authors.
E-mail addresses: luodong@jnu.edu.cn (D. Luo), zhouxp@jnu.edu.cn (X.-P. Zhou).

https://doi.org/10.1016/j.cclet.2025.111331
1001-8417/© 2026 Published by Elsevier B.V. on behalf of Chinese Chemical Society and Institute of Materia Medica, Chinese Academy of Medical Sciences.

system with the ability to responsively release guests [35]. The development of such cage systems in which topology is maintained after vertex modifications will provide an excellent platform for studying attractive host-guest chemistry.

Here, we explore a vertex functionalization method to study the influences of the host-guest chemistry of MOCs by comparing fluorinated hexahedral MOC **1** and non-fluorinated MOC **2** [40,41]. Structural characterization *via* single-crystal X-ray diffraction (SCXRD), ^{1}H nuclear magnetic resonance (NMR) spectra, electrospray ionization time-of-flight mass spectra (ESI-TOF MS) confirmed that MOC **1** adopts low-symmetry architectures similar to MOC **2**, with fluorine atoms positioned at cage windows. ^{1}H/^{19}F NMR spectra of **1·NTf$_2$** and **1·OTf** exhibited slow-exchange binding behavior on the NMR time scale with the external anions. The ^{1}H NMR spectrum of **1·NTf$_2$** showed a single set of peaks in the imine signal area, while **1·OTf** displayed two distinct groups of signals. This suggests that the NTf_2^- anion has a stronger binding affinity with the cage. Competitive anion titrations also demonstrated a hierarchy in binding strength (NTf_2^- > OTf^- > BF_4^-), with NTf_2^- resisting displacement by smaller anions or aromatic guests. Host-guest studies showed pyrene fully displaced OTf^- but not NTf_2^-, underscoring the superior affinity of NTf_2^-. Isothermal titration calorimetry (ITC) further revealed reduced association constants for **1·OTf** compared to **2·OTf** when binding polycyclic hydrocarbons. This was attributed to the electron-withdrawing fluorine effects altering charge distribution. These findings highlight how vertex modification fine-tunes anion selectivity and guest-binding thermodynamics in MOCs, offering a strategic approach to designing adaptive supramolecular hosts for applications.

The reaction of 1,2,4,5-tetrakis-(4-aminolphenyl)benzene (TAPB), 3-fluoro-2-formylpyridine, and ZnX_2 (X including NTf_2^-, OTf^-, and BF_4^-) salt in acetonitrile (CH_3CN) at 70 °C for 8 h gave MOC **1** (Fig. 1, see Supporting information for synthesis experimental details). The products corresponding to different counteracting anions were named as **1·NTf$_2$**, **1·OTf**, and **1·BF$_4$**. As comparative structures with the same geometric shape, the previously reported MOC **2** (marked as **2·OTf**, **2·NTf$_2$**, and **2·BF$_4$**) [40,41] was synthesized by replacing 3-fluoro-2-formylpyridine with 2-formylpyridine in the former synthesis conditions. The ^{1}H NMR spectra of MOCs **1** and **2** were recorded and showed in Fig. 2, Figs. S3, S13, S25, and S35-S37 (Supporting information). The ^{1}H NMR spectrum of **1·NTf$_2$** in CD_3CN displayed four distinct signals in the imine region with integrated area ratio of 1:1:1:1 (H_1, Fig. 2), which are similar to the signals of **2·NTf$_2$**, indicating that they may have similar low-symmetry cage structures [41]. However, it is evident that the ^{1}H NMR signal distribution of **1·OTf** was significantly different from that of **2·OTf**. Eight signals appeared in the imine region, and their integrated area ratios were 1:1:1:1:1:1:1:1 (Fig. 2), suggesting that they might belong to two different forms of cage species in the solution. The similar results appeared in the ^{1}H NMR spectra of **1·BF$_4$** after comparison with **2·BF$_4$** (Fig. 2). The above phenomenon prompted us to speculate that the modification of the cage vertices resulted in a significant change in the host-guest binding behavior between the cage and the anions.

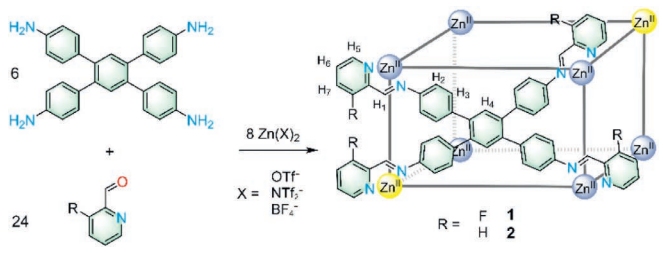


Fig. 1. Schematic diagram showing the self-assembly of hexahedral MOC **1** and **2**. The purple and yellow vertices represent two different stereochemical centers.

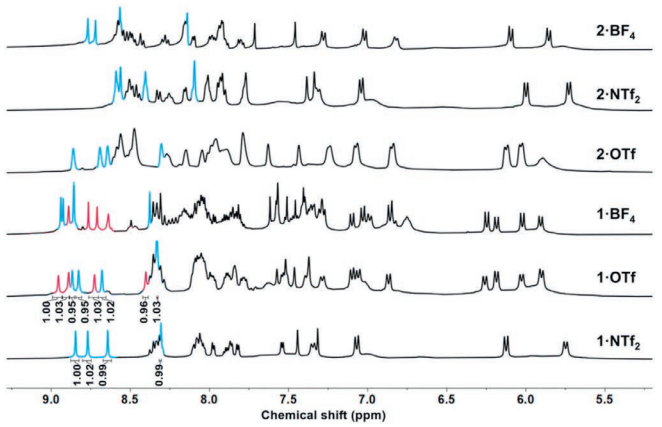


Fig. 2. ^{1}H NMR spectra of MOC **1·NTf$_2$**, **1·OTf**, **1·BF$_4$**, **2·OTf**, **2·NTf$_2$**, and **2·BF$_4$**, respectively (CD_3CN, 400 MHz, 298 K). The blue peaks in the aromatic region correspond to the imine hydrogen atoms of the cages bound to anions in solution, while the red peaks represent the imine hydrogen atoms of the cages not bound to anions in solution.

In order to understand the reasons for the differences in the above ^{1}H NMR data, **1·NTf$_2$** and **1·OTf** were selected as key research objects for detailed characterization. The diffusion ordered ^{1}H NMR spectrum (DOSY) and ESI-TOF MS were firstly measured to investigate the composition of **1·NTf$_2$**. As showed in Fig. S4 (Supporting information), all the peaks of **1·NTf$_2$** had the same diffusion constant ($D = 5.50 \times 10^{-10}$ m^2/s), indicating that these peaks belonged to a single species. The hydrodynamic radius of **1·NTf$_2$** in CH_3CN was calculated to be ~11.9 Å *via* the Stokes-Einstein equation [42,43]. At the same time, ESI-TOF mass spectra (Figs. S5 and S6 in Supporting information) showed that **1·NTf$_2$** had multi-charge features and the compositional characteristic of $[Zn_8L_6(NTf_2)_{16-n}]^{n+}$ (n = 10–4). The main peak observed at m/z = 1181.0524 matched the $[\mathbf{1}\cdot(NTf_2)_9]^{7+}$ species (calculated value 1180.9854). Additionally, all peaks corresponding to the different charged species aligned well with their calculated isotopic patterns, confirming the composition and stability of **1·NTf$_2$** in the CH_3CN solution. In addition, purple block crystals of **1·NTf$_2$** that suitable for single crystal X-ray diffraction (SCXRD) analysis were obtained by diffusing ethyl acetate vapor into its CH_3CN solution containing iodine as crystallization-aiding molecules (see Supporting information for detailed crystallographic data). **1·NTf$_2$** crystallizes in the monoclinic space group $P2_1/c$, and the cage molecule features an 8-nucleus hexahedral structure (Fig. 3a). Six TAPB-based ligands act as faces of the cage with an average distance of about 12.25 Å between the face centers, bridging the eight octahedral Zn^{II} centers and forming ΔΔΔΔΔΔΔΔ or ΛΛΔΔΔΔΔΔ stereo configurations, which are similar to that of **2·NTf$_2$** (Fig. 3b) [41]. The hydrophobic cavities of **1·NTf$_2$** and **2·NTf$_2$** have the volume of 492 Å^3 and 482 Å^3, respectively, estimated by MoloVol with a probe radius of 1.2 Å [41]. It is worth noting that the modified fluorine atoms on the ligand surround the vertex and are arranged at the window of **1·NTf$_2$** (Fig. 3). These structural features may have an impact on its host-guest behavior.

Subsequently, a variety of 2D NMR spectra were utilized to validate the structure of **1·NTf$_2$** in solution (Figs. S8-S10 in Supporting information). The heteronuclear single quantum correlation (HSQC) spectrum of **1·NTf$_2$** (Fig. S8) showed that there was one set of imine signals belonging to the cage species in the imine region. Moreover, the ^{19}F NMR spectrum of **1·NTf$_2$** was recorded and showed two sets of signal distribution (Fig. S11 in Supporting information). From the region of −119 ~ −122 ppm, there were four

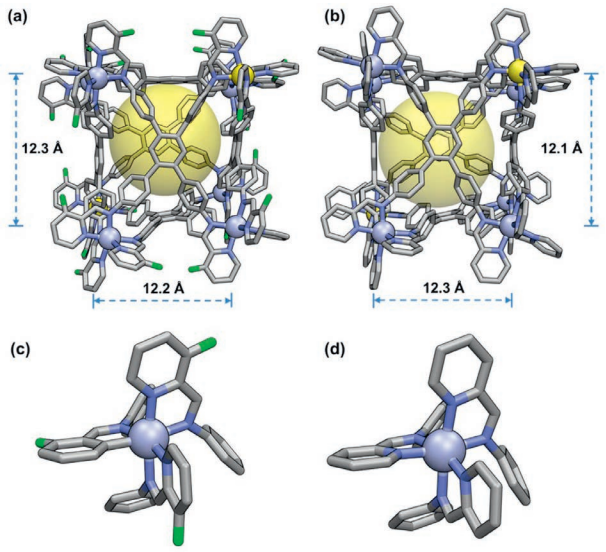


Fig. 3. Single crystal structure of hexahedral cages of (a) **1·NTf** and (b) **2·NTf$_2$**. Coordination environment with Δ-configured Zn vertices in cages (c) **1·NTf** and (d) **2·NTf$_2$**. Color codes: Zn light purple (Δ configuration) or yellow (Λ configuration), C gray, N blue, F green. The transparent yellow ball represents the cavity in the cage. The anions and hydrogen atoms were hidden for clarity.

different F signals attributed to pyridine parts, and their integrated area ratio was 1:1:1:1. It was consistent with the situation of imine signals, further proving that **1·NTf$_2$** had a low symmetry structure. Another group of signals came from NTf_2^- anions. It was found that the peaks at −70.4 and −80.1 ppm corresponded to encapsulated and free NTf_2^- anions respectively [44]. Based on the above data, it can be concluded that there is a host-guest binding between the cage and the NTf_2^- anion, and this process exhibits slow exchange on the nuclear magnetic time scale [34,44–46] without affected by temperature (Fig. S12 in Supporting information).

Similar characterizations were performed on **1·OTf** to explore its different host-guest binding behaviors. The DOSY ^{1}H NMR spectrum and ESI-TOF MS of **1·OTf** were tested and showed in Fig. S14 (Supporting information). All the peaks of **1·OTf** had the same diffusion constant ($D = 3.54 \times 10^{-10}$ m^2/s). At the same time, ESI-TOF mass spectra (Figs. S15 and S16 in Supporting information) of **1·OTf** had multi-charge species and the compositional characteristic of $[Zn_8L_6(OTf)_{16-n}]^{n+}$ ($n = 9$–4). The main peak observed at $m/z = 1012.8159$ matched the $[\mathbf{1}\cdot(OTf)_9]^{7+}$ species (calculated value 1012.8835). All signals attributed to the various charged species matched their calculated isotopic patterns. Furthermore, several 2D NMR spectra were examined (Figs. S18-S20 in Supporting information), including the HSQC spectrum of **1·OTf** (Fig. S18), which revealed two distinct sets of imine signals corresponding to different cage species in the imine region. The ^{19}F NMR spectrum of **1·OTf** was shown in Fig. S21 (Supporting information). The presence of two groups of signals in the range of −119 ∼ −122 ppm also supported the inference that there were two different species in the solution. The signal at −78.25 ppm indicated that some of OTf^- anions were encapsulated in the cage. Additionally, the ^{1}H NMR spectra of **1·OTf** with varying concentrations and temperatures (Figs. S22-S24 in Supporting information) indicated that the composition of species in the solution was minimally influenced by these factors. More importantly, the crystal structure of **1·OTf** (see Supporting information for detailed crystallographic data) shows that it has a similar structure to **1·NTf$_2$**, indicating that the differences between the two species mentioned above are caused by the host-guest interactions between the cage and anions, rather than the symmetry or a new structure of the cage. Therefore, we speculate that **1·OTf** has the same cage skeleton as **1·NTf$_2$**, but the complex ^{1}H NMR spectrum (Fig. 2) should be caused by the different degrees of slow exchange process between OTf^- and the cage on the NMR time scale [44–46]. The binding behavior of **1·OTf** is different from **1·NTf$_2$**, **2·OTf**, and **2·NTf$_2$**, indicating that through vertex modification, MOC **1** has acquired the ability to selectively bind with anionic guests.

To further investigate the changes in binding ability between anionic guests and metal-organic cages caused by vertex modifications, we performed a series of experiments involving anion titrations. The general procedure involves dissolving **1·NTf$_2$** or **1·OTf** in CD_3CN (2.5×10^{-3} mol/L), followed by the addition of 16 equiv. of tetrabutylammonium trifluoromethanesulfonate (TBAOTf) or tetrabutylammonium bis((trifluoromethyl)sulfonyl)amide ($TBANTf_2$), respectively. The solutions were equilibrated at 70 °C for 3 h, and then the system was characterized by ^{1}H NMR and ^{19}F NMR. As shown in Fig. 4a and Fig. S40 (Supporting information), with the addition of 16 equiv. of OTf^- anion, there is no change in the aromatic region of the ^{1}H NMR spectra of **1·NTf$_2$**. Additionally, the ^{19}F NMR spectra of the system (marked as **TBAOTf@1·NTf$_2$**, Fig. 4b) indicate that in the range of −79 ∼ −80 ppm, upon the addition of OTf^- anion, the bound NTf_2^- anions remain unchanged and there are no signals indicating the presence of encapsulated OTf^- anion. Furthermore, the chemical environment of the fluorine atoms on the cage remains consistent (Fig. S41 in Supporting information). These initial findings suggest that the MOC **1** has a higher binding affinity for NTf_2^- anions compared to OTf^- anions. To further validate this result, the **1·OTf** solution was titrated with NTf_2^- anions. As shown in Figs. 4c and d, the addition of NTf_2^- anions has resulted in significant changes in the ^{1}H and ^{19}F NMR spectra of the system (marked as **TBANTf$_2$@1·OTf**). With the addition of NTf_2^- anions, the original two sets of signals of **1·OTf** (Fig. 4c) gradually merged into a single group, and at the endpoint of titration, the ^{1}H NMR spectrum of the system was closely matched with that of **1·NTf$_2$** (Fig. S43 in Supporting information). Moreover, the ^{19}F NMR spectra of **TBANTf$_2$@1·OTf** (Fig. 4d and Fig. S44 in Supporting information) showed that the signals of the bound OTf^- anions on the cage diminish gradually, and the introduced NTf_2^- anions take their place. These results suggest that NTf_2^- anions are able to fully replace the bound OTf^- anions and also verify that NTf_2^- anion has a stronger binding ability with MOC **1**.

Since the NTf_2^- anion is larger than the OTf^- anion, which may impact its ability to bind to the cage [44], we opted to conduct titration experiments using the smaller BF_4^- anion to validate this hypothesis. First, the BF_4^- anions were titrated into the **1·NTf$_2$** solution (marked as **TBABF$_4$@1·NTf$_2$**), and the ^{1}H and ^{19}F NMR spectra of this process were recorded. As shown in Fig. S43, after adding 16 equiv. of BF_4^- anions, the ^{1}H NMR spectra of **TBABF$_4$@1·NTf$_2$** remained almost unchanged. Additionally, the ^{19}F NMR spectra of **TBABF$_4$@1·NTf$_2$** (Fig. S45 in Supporting information) clearly revealed that the encapsulated NTf_2^- anions were not displaced by BF_4^- anions, and there was no obvious signal of encapsulated BF_4^- anions. This proves that the binding ability of the cage to NTf_2^- anion is indeed stronger than that of BF_4^- anion. Next, the same titration procedure and characterization was used for the **TBABF$_4$@1·OTf** system (Figs. S47 and S48 in Supporting information). As BF_4^- anions were gradually added, the peak in the imine hydrogen region of **TBABF$_4$@1·OTf** showed a slight change. This may be caused by the replacement of some OTf^- anions, which was confirmed by the ^{19}F NMR spectra of the system. The originally encapsulated OTf^- anions in **1·OTf** were partially replaced. When 16 equiv. of BF_4^- anion were added, this replacement still did not reach equilibrium. These results reveal that under the same concentration, the binding ability of OTf^- anion to the cage is still stronger than that of BF_4^- anion. The above titration experiments generally reveal that NTf_2^- anion

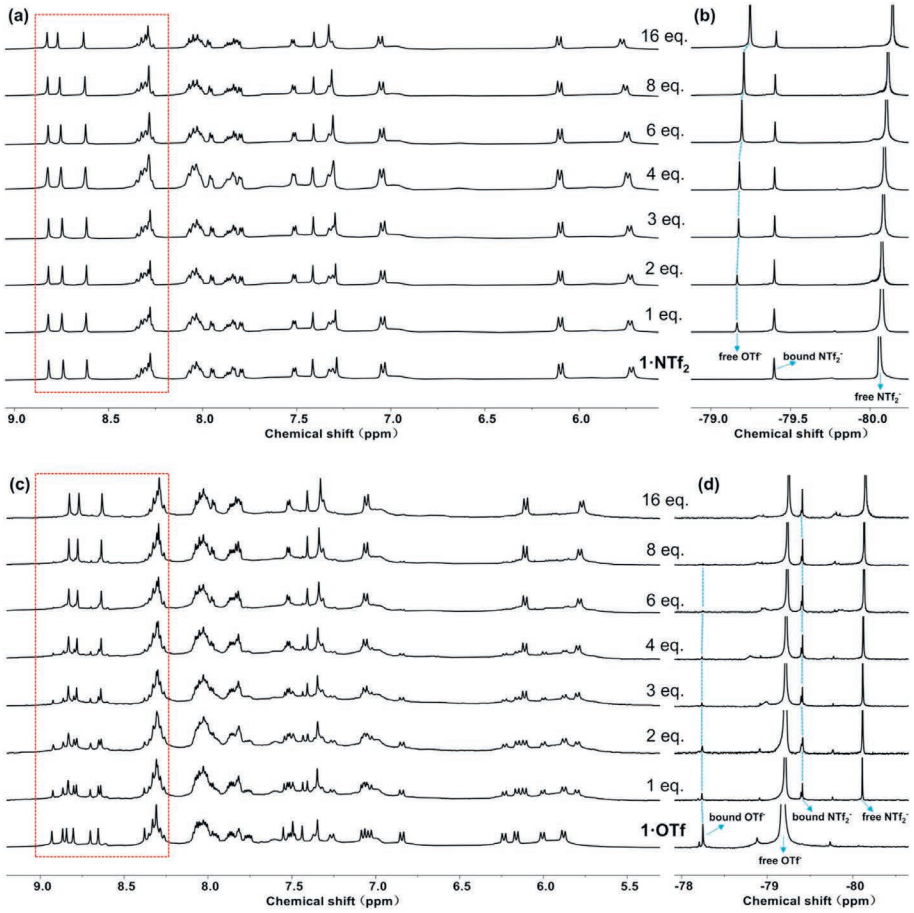


Fig. 4. (a) Aromatic region of the ^{1}H NMR spectra (CD_3CN, 400 MHz, 298 K) and (b) ^{19}F NMR spectra (CD_3CN, 376 MHz, 298 K) of **1·NTf$_2$** (2.5×10^{-3} mol/L) titrated with 16 equiv. of TBAOTf. (c) Aromatic region of ^{1}H NMR spectra (CD_3CN, 400 MHz, 298 K) and (d) ^{19}F NMR spectra (CD_3CN, 376 MHz, 298 K) of **1·OTf** (2.5×10^{-3} mol/L) titrated with 16 equiv. of $TBANTf_2$. The red box area shows the changes in the imine hydrogen NMR signals during the titration process. The blue dashed line represents the variation in NMR signals of fluoride atoms present in the anions as the titration progresses.

Table 1
ITC data of **1·NTf$_2$** and **1·OTf** (1.0×10^{-3} mol/L) titrated with TBAOTf, $TBANTf_2$, and $TBABF_4$ (20×10^{-3} mol/L) in CH_3CN, respectively.

Sample	K (10^3 L/mol)	$\triangle G$ (kcal/mol)	$\triangle H$ (kcal/mol)	$T\triangle S$ (kcal/mol)
TBAOTf@1·NTf$_2$	/	/	/	/
TBANTf$_2$@1·OTf	1.314 ± 0.149	−0.196	0.290 ± 0.024	0.486
TBABF$_4$@1·NTf$_2$	0.254 ± 0.120	−0.124	0.392 ± 0.111	0.516
TBABF$_4$@1·OTf	0.413 ± 0.054	−0.312	0.174 ± 0.034	0.486

with larger size and charge distribution area may have stronger host-guest interactions with the cage.

The isothermal titration calorimetry (ITC) technology is often used to study the association constants and thermodynamic parameters involved in forming host-guest complexes, which is important for understanding the binding process between host and guest [47–50]. Upon the addition of TBAOTf, $TBANTf_2$, or $TBABF_4$ (20×10^{-3} mol/L) to a CH_3CN solution of **1·NTf$_2$** or **1·OTf** (1.0×10^{-3} mol/L), the association constants and thermodynamic parameters of these processes could be obtained and showed in Figs. S51 and S52 (Supporting information) and Table 1. Comparing and analyzing the experimental results, we observed that the association constant (K) value of the **TBANTf$_2$@1·OTf** system was the highest at 1.314×10^3 L/mol, while the corresponding **TBAOTf@1·NTf$_2$** system did not exhibit significant heat exchange. This finding indicates that **1·OTf** can convert to **1·NTf$_2$** during the titration process with $TBANTf_2$, whereas **1·NTf$_2$** remains unchanged during the titration process with TBAOTf. This result is highly consistent with the NMR titration data. It is worth noting that in the **TBANTf$_2$@1·OTf** system, the $\triangle H$ and $T\triangle S$ values are 0.290 and 0.486 kcal/mol, respectively, indicating that the complexation process is driven by entropy. Additionally, the K value of **TBABF$_4$@1·NTf$_2$** system is 0.254×10^3 L/mol, which suggests that there could be some anion exchange processes occurring in the system. However, due to the entropy-driven nature of the above processes, they exhibit slight variations from the NMR results.

In our previous work [40], we have already demonstrated the selective encapsulation properties of the MOC **2** for pyrene. Hence, we are interested in investigating whether the binding ability of MOC **1** to pyrene is altered following vertex modification. To broaden the scope of our experiments, pyrene (Py) and its analogs 4,5,9,10-tetrahydropyrene (4H-Py) and hexadecahydropyrene (16H-Py) were selected as guests for binding test. In two standard experiments, **1·NTf$_2$** and **1·OTf** were dissolved in CH_3CN (0.4 mL, 0.001 mmol), respectively, and an excess (5 equiv.) of pyrene was added to each solution. The reaction systems were equilibrated at 70 °C for 3 h. The reaction products were analyzed by NMR spectra (^{1}H NMR, ^{19}F NMR, COSY, NOESY, and DOSY, see Supporting information for details). As shown in Fig. 5a, most signals of **1·NTf$_2$** remained unchanged, and a new set of characteristic peaks corresponding to **Py@1·NTf$_2$** emerged, which was also confirmed by ESI-TOF mass spectrum (Fig. S56 in Supporting information). It was worth noting that the ^{19}F NMR spectra (Fig. 5b) of the NTf_2^- anions encapsulated in the cage did not change significantly before and after encapsulation of pyrene. The results indicate that the

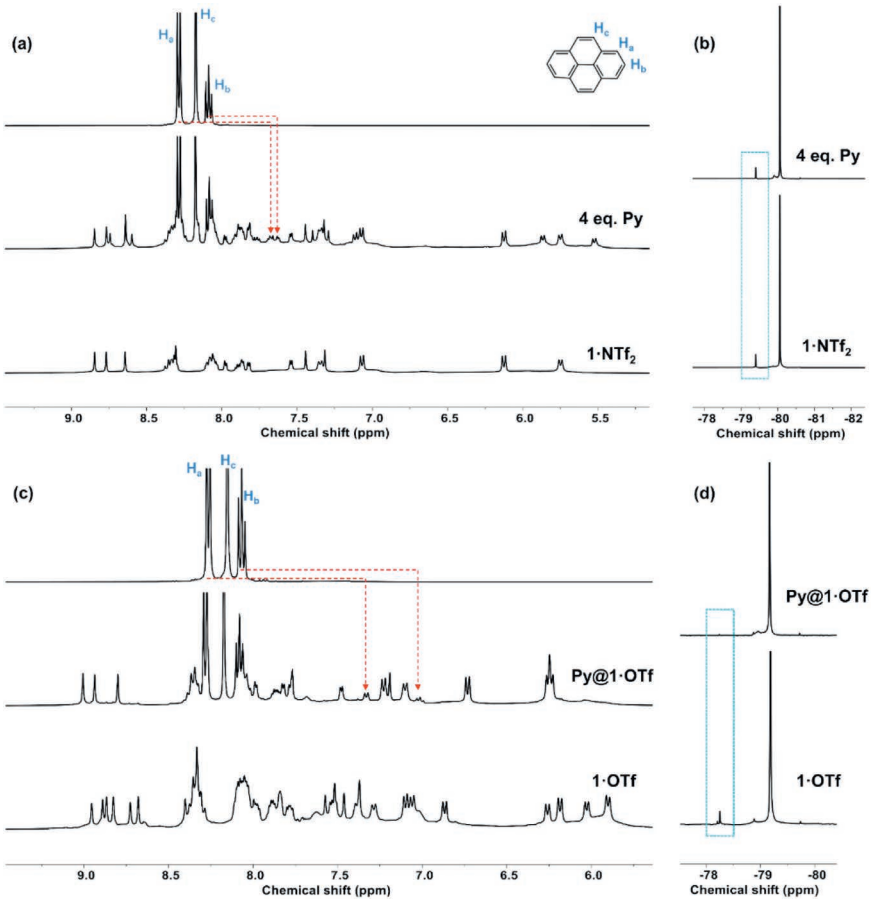


Fig. 5. (a) Aromatic region of the ^{1}H NMR spectra (CD_3CN, 400 MHz, 298 K) and (b) ^{19}F NMR spectra (CD_3CN, 376 MHz, 298 K) of **1·NTf$_2$** (2.5×10^{-3} mol/L) titrated with 4 equiv. of Py. (c) Aromatic region of ^{1}H NMR spectra (CD_3CN, 400 MHz, 298 K) and (d) ^{19}F NMR spectra (CD_3CN, 376 MHz, 298 K) of **1·OTf** (2.5×10^{-3} mol/L) titrated with 4 equiv. of Py. The red dashed line shows the changes in Py hydrogen NMR signals after the titration process. The blue box area represents the variation in NMR signals of fluoride atoms present in the anions as the titration progresses.

NTf_2^- anions have a stronger binding affinity with the cage than pyrene molecules. In comparison, the ^{1}H NMR spectra of **Py@1·OTf** (Fig. 5c) exhibited noticeable shifts in either the high-field or low-field regions upon pyrene encapsulation compared to **1·OTf**. It was observed that the two sets of signals for imine atoms of **1·OTf** merged into single group. Upon the release of the encapsulated OTf^- anions (Fig. 5d), the signals for F also merged into a single set (Fig. S66 in Supporting information), indicating complete replacement of the encapsulated OTf^- anions. The ESI-TOF mass spectrum results also supported that the cage cavity was completely occupied by pyrene with the molar ratio of 1:1 for the host-guest complex (Fig. S70 in Supporting information). When pyrene is replaced by 4H-Py and 16H-Py, similar results can be obtained (see Supporting information for details). Overall, the host-guest chemistry experiments involving pyrene and its analogs further confirmed the stronger binding interaction between NTf_2^- anion and the cage compared to OTf^- anion.

Since these polycyclic hydrocarbon guests can completely displace OTf^- anions from the cage, it is beneficial to use ITC technology to study the thermodynamic parameters and association constants in these processes. **1·OTf** and **2·OTf** were selected as host molecules for subsequent testing. The ITC data were displayed in Figs. S92-S94 (Supporting information) and Table 2. All guest exchange processes are exothermic processes, indicating that they are driven by enthalpy. From the data listed in Table 2, Py and its analogs form complexes with **1·OTf**, and their association constants follow the order: K(**Py@1·OTf**) > K(**4H-Py@1·OTf**) > K(**16H-Py@1·OTf**). The same trend is observed for the complexes with **2·OTf**. Additionally, the time-dependent ^{1}H NMR spectra of the binding process between **1·OTf** or **2·OTf** and Py or its analogs were recorded (Figs. S95-S100 in Supporting information). The results indicate that the system reaches equilibrium at 5 min after adding pyrene to the **1·OTf** solution. In comparison, the corresponding equilibrium times for the 4H-Py and 16H-Py systems are 1 h and >2 h, respectively. The host-guest system corresponding to **2·OTf** shows a kinetic encapsulation process similar to that of **1·OTf**. These can be attributed to the fact that Py has a larger π electron delocalization structure, which can form stronger C–H$\cdots\pi$ interactions with the cage skeleton [40]. However, due to partial hydrogenation, the aromaticity of 4H-Py is reduced, resulting in a decrease in the number of binding sites and strength. Fully hydrogenated 16H-Py lacks a conjugated system, has a more flexible structure and weaker binding ability. It is worth noting that

Table 2
ITC data of **1·OTf** and **2·OTf** (1.0×10^{-3} mol/L) titrated with Py, 4H-Py, and 16H-Py (20.0×10^{-3} mol/L) in CH_3CN, respectively.

Sample	K (10^3 L/mol)	$\triangle G$ (kcal/mol)	$\triangle H$ (kcal/mol)	$T\triangle S$ (kcal/mol)
Py@1·OTf	0.921 ± 0.211	−0.683	−0.350 ± 0.025	0.333
Py@2·OTf	1.11 ± 0.107	−1.14	−0.798 ± 0.059	0.339
4H-Py@1·OTf	0.705 ± 0.089	−1.27	−0.845 ± 0.146	0.429
4H-Py@2·OTf	0.905 ± 0.215	−1.15	−0.752 ± 0.026	0.396
16H-Py@1·OTf	0.155 ± 0.068	−1.23	−0.848 ± 0.243	0.384
16H-Py@2·OTf	0.201 ± 0.051	−0.558	−0.117 ± 0.047	0.441

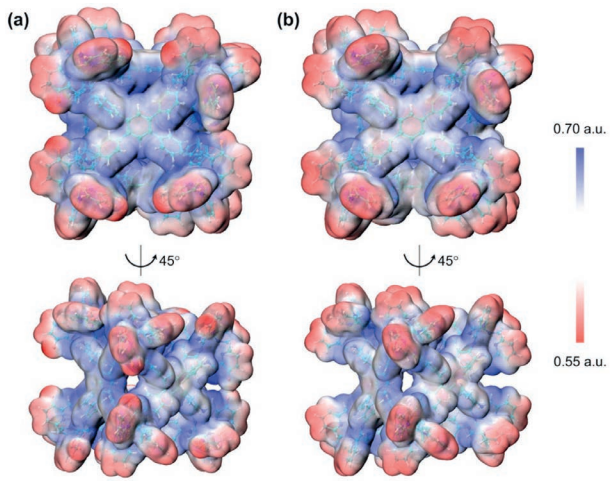


Fig. 6. The electrostatic potential analysis on van der Waals surface of skeleton of (a) MOC **1** and (b) MOC **2**. The blue and red area represent the relative positive and negative charge distribution.

there are significant differences in the binding constants for the formation of host-guest complexes with the same guest molecule, as seen in **1·OTf** and **2·OTf**. Taking Py as an example, its association constant with **1·OTf** is 0.921×10^3 L/mol, and with **2·OTf** it is 1.11×10^3 L/mol, the latter being greater than the former. The same situation occurs when 4H-Py and 16H-Py are guests. This may be due to the electron-withdrawing nature of the fluorine atoms introduced by the vertex modification, which changes the overall charge distribution of MOC **1** skeleton, weakening its interaction with Py and its analogs. To verify this speculation, electrostatic potential (ESP) analysis based on density functional theory (DFT) calculations was performed to probe the effect of F substitution on the charge distribution of the skeletons of MOC **1** and **2**. As illustrated in Fig. 6, the positively charged areas at the face and window positions of MOC **1** are more extensive and intense than those of MOC **2**, indicating that the F substitution induced a decrease in the electron density of the cage skeleton. The above changes lead to a weakening of the C–H$\cdots\pi$ interaction between the guest and the MOC **1** skeleton [40], which is manifested as a binding constant smaller than that of the corresponding MOC **2**.

In summary, we demonstrate a feasible vertex modification approach for tuning the host-guest chemistry of metal-organic cages. The vertex modification of MOC **1** with fluorine atoms significantly alters its host-guest chemistry compared to the non-fluorinated analog MOC **2**. Structural and spectroscopic analyses confirmed that MOC **1** retains a hexahedral skeleton but exhibits enhanced anion selectivity, favoring larger NTf_2^- over OTf^- or BF_4^-. Furthermore, pyrene displaced OTf^- but not NTf_2^-, reflecting the hierarchical binding strengths of anions. The reduced association constants of **1·OTf** with pyrene and its analogs, compared to **2·OTf**, highlight the electronic effects of fluorine substitution on host-guest affinity. This work demonstrates that strategic vertex modification in MOCs enables fine-tuning of anion selectivity and guest-binding properties. This approach offers valuable insights for creating new functional materials based on metal-organic cages for applications such as molecular recognition, sensing, and catalysis in the future.

CRediT authorship contribution statement

Tian Tan: Writing – review & editing, Writing – original draft, Investigation, Data curation. **Jiao Hu:** Writing – review & editing, Software, Investigation, Data curation. **Ya-Liang Lai:** Writing – review & editing, Validation, Software, Data curation. **Xian-Chao Zhou:** Writing – review & editing, Visualization, Validation, Data curation. **Yong-Zhen Tan:** Writing – review & editing, Software, Data curation. **Mo Xie:** Writing – review & editing, Software, Formal analysis. **Yong-Liang Huang:** Writing – review & editing, Software, Data curation. **Chuang-Wei Zhou:** Writing – review & editing, Software, Data curation. **Hao-Jie Zhang:** Writing – review & editing, Validation, Data curation. **Dong Luo:** Writing – review & editing, Writing – original draft, Supervision, Resources, Methodology, Investigation, Funding acquisition, Data curation, Conceptualization. **Xiao-Ping Zhou:** Writing – review & editing, Supervision, Resources, Investigation, Funding acquisition, Conceptualization. **Dan Li:** Writing – review & editing, Supervision, Resources, Funding acquisition.

Declaration of competing interest

The authors declare that they have no known competing financial interests or personal relationships that could have appeared to influence the work reported in this paper.

Acknowledgments

This work was financially supported by the National Natural Science Foundation of China (Nos. 22375075, 22171106, 22201101, and 22471098), the Guangdong Major Project of Basic and Applied Research (No. 2019B030302009), the Guangdong Basic and Applied Basic Research Foundation (Nos. 2022A1515011937, 2024A1515011753, 2025A1515012169), the Youth Enhancement Program of Guangdong Basic and Applied Research (No. 2023A1515030234), and the Guangzhou Science and Technology Program (No. 2025A04J3411). We thank the high-performance public computing service platform of Jinan University for providing computational resources.

Supplementary materials

Supplementary material associated with this article can be found, in the online version, at doi:10.1016/j.cclet.2025.111331.

References

[1] M. Fujita, M. Tominaga, A. Hori, B. Therrien, Acc. Chem. Res. 38 (2005) 371–380.
[2] M.D. Pluth, K.N. Raymond, Chem. Soc. Rev. 36 (2007) 161–171.
[3] T.R. Cook, P.J. Stang, Chem. Rev. 115 (2015) 7001–7045.
[4] F.J. Rizzuto, L.K.S. von Krbek, J.R. Nitschke, Nat. Rev. Chem. 3 (2019) 204–222.
[5] M. Han, D.M. Engelhard, G.H. Clever, Chem. Soc. Rev. 43 (2014) 1848–1860.
[6] Y.L. Lu, Y.P. Wang, K. Wu, M. Pan, C.Y. Su, Acc. Chem. Res. 57 (2024) 3277–3291.
[7] Y. Jin, Q. Zhang, Y. Zhang, C. Duan, Chem. Soc. Rev. 49 (2020) 5561–5600 49.
[8] X.Z. Li, C.B. Tian, Q.F. Sun, Chem. Rev. 122 (2022) 6374–6458.
[9] H. Amouri, C. Desmarets, J. Moussa, Chem. Rev. 112 (2012) 2015–2041.
[10] A. Ghosh, J. Pruchyathamkorn, C.F. Espinosa, J.R. Nitschke, J. Am. Chem. Soc. 146 (2024) 2568–2573.
[11] E. Benchimol, H.M. O'Connor, B. Schmidt, et al., Angew. Chem. Int. Ed. 64 (2025) e202421137.
[12] C.W. Zhou, X.Z. Wang, M. Xie, et al., Angew. Chem. Int. Ed. 62 (2023) e202315020.
[13] P. Mal, B. Breiner, K. Rissanen, J.R. Nitschke, Science 324 (2009) 1697–1699.
[14] M. Yamashina, Y. Sei, M. Akita, M. Yoshizawa, Nat. Commun. 5 (2014) 4662.
[15] H. Takezawa, K. Shitozawa, M. Fujita, Nat. Chem. 12 (2020) 574–578.
[16] C.J. Brown, F.D. Toste, R.G. Bergman, K.N. Raymond, Chem. Rev. 115 (2015) 3012–3035.
[17] S.H.A.M. Leenders, R. Gramage-Doria, B. de Bruin, J.N.H. Reek, Chem. Soc. Rev. 44 (2015) 433–448.
[18] J. Jiao, Z. Li, Z. Qiao, et al., Nat. Commun. 9 (2018) 4423.
[19] Y.-P. Wang, Y. Zhang, X.H. Duan, et al., Coord. Chem. Rev. 501 (2024) 215570.
[20] E.G. Percastegui, T.K. Ronson, J.R. Nitschke, Chem. Rev. 120 (2020) 13480–13544.
[21] M.M.J. Smulders, I.A. Riddell, C. Browne, J.R. Nitschke, Chem. Soc. Rev. 42 (2013) 1728–1754.
[22] R. Custelcean, Chem. Soc. Rev. 43 (2014) 1813–1824.
[23] X.W. Zhu, D. Luo, X.P. Zhou, D. Li, Coord. Chem. Rev. 455 (2022) 214354.
[24] D.A. Roberts, B.S. Pilgrim, J.R. Nitschke, Chem. Soc. Rev. 47 (2018) 626–644.
[25] S. Pullen, G.H. Clever, Acc. Chem. Res. 51 (2018) 3052–3064.

[26] E. Sanchez-Gonzalez, M.Y. Tsang, J. Troyano, G.A. Craig, S. Furukawa, Chem. Soc. Rev. 51 (2022) 4876–4889.
[27] J. Liu, Z. Wang, P. Cheng, et al., Nat. Rev. Chem. 6 (2022) 339–356.
[28] D. Luo, X.W. Zhu, X.P. Zhou, D. Li, Chem. Eur. J. 30 (2024) e202400020.
[29] D. Fujita, Y. Ueda, S. Sato, et al., Chem 1 (2016) 91–101.
[30] B. Chen, J.J. Holstein, A. Platzek, et al., Chem. Sci. 13 (2022) 1829–1834.
[31] Y. Liu, S.H. Liao, W.T. Dai, et al., Angew. Chem. Int. Ed. 62 (2023) e202217215.
[32] D. Luo, X.Z. Wang, C. Yang, X.P. Zhou, D. Li, J. Am. Chem. Soc. 140 (2018) 118–121.
[33] W. Xue, K. Wu, N. Ouyang, et al., Angew. Chem. Int. Ed. 62 (2023) e202301319.
[34] H. Zhu, T.K. Ronson, K. Wu, J.R. Nitschke, J. Am. Chem. Soc. 146 (2024) 2370–2378.
[35] A.J. McConnell, C.M. Aitchison, A.B. Grommet, J.R. Nitschke, J. Am. Chem. Soc. 139 (2017) 6294–6297.
[36] Y. Yang, T.K. Ronson, J. Zheng, N. Mihara, J.R. Nitschke, Chem 9 (2023) 1972–1982.
[37] M.D. Ludden, C.G.P. Taylor, M.D. Ward, Chem. Sci. 12 (2021) 12640–12650.
[38] X. Zhang, X. Dong, W. Lu, et al., J. Am. Chem. Soc. 141 (2019) 11621–11627.
[39] M.Y. Sun, M. Xie, C.W. Zhou, Sci. China Chem. 66 (2023) 2004–2010.
[40] Y.L. Lai, J. Su, L.X. Wu, et al., Chin. Chem. Lett. 35 (2024) 108326.
[41] J.A. Davies, A. Tarzia, T.K. Ronson, et al., Angew. Chem. Int. Ed. 62 (2023) e202217987.
[42] D. Luo, L.X. Wu, Y. Zhang, et al., Sci. China Chem. 65 (2022) 1105–1111.
[43] D. Luo, Z.J. Yuan, L.J. Ping, et al., Angew. Chem. Int. Ed. 62 (2023) e202216977.
[44] D. Zhang, T.K. Ronson, J. Mosquera, et al., J. Am. Chem. Soc. 139 (2017) 6574–6577.
[45] S. Ma, M.M.J. Smulders, Y.R. Hristova, et al., J. Am. Chem. Soc. 135 (2013) 5678–5684.
[46] M.M.J. Smulders, S. Zarra, J.R. Nitschke, J. Am. Chem. Soc. 135 (2013) 7039–7046.
[47] Y.L. Lai, M. Xie, X.C. Zhou, et al., Angew. Chem. Int. Ed. 63 (2024) e202402829.
[48] G. Li, T.K. Ronson, R. Lavendomme, et al., Chem 9 (2023) 1549–1561.
[49] R.J. Li, M. Han, J. Tessarolo, et al., ChemPhotoChem 3 (2019) 378–383.
[50] T. Feng, X. Li, J. Wu, C. He, C. Duan, Chin. Chem. Lett. 31 (2020) 95–98.